THE JOURNAL OF PHYSICAL CHEMISTRY C

Article

pubs.acs.org/JPCC

Probing the Quenching of Quantum Dot Photoluminescence by Peptide-Labeled Ruthenium(II) Complexes

Amy M. Scott,*[,†] W. Russ Algar,[‡,▽] Michael H. Stewart,[§] Scott A. Trammell,[‡] Juan B. Blanco-Canosa,[⊥] Philip E. Dawson,[⊥] Jeffrey R. Deschamps,[‡] Ramasis Goswami,[∥] Eunkeu Oh,[§,#] Alan L. Huston,[§] and Igor L. Medintz*[,‡]

[†]Department of Chemistry, University of Miami, 1301 Memorial Drive, Miami, Florida 33146, United States

[‡]Center for Bio/Molecular Science and Engineering, Code 6900, [§]Optical Sciences Division, Code 5611, and [∥]Material Sciences and Technology, Code 6351, U.S. Naval Research Laboratory, Washington, DC 20375, United States

[⊥]Departments of Cell Biology and Chemistry, The Scripps Research Institute, La Jolla, California 92037, United States

[#]Sotera Defense Solutions, Columbia, Maryland 21046, United States

Supporting Information

ABSTRACT: Charge transfer processes with semiconductor quantum dots (QDs) have generated much interest for potential utility in energy conversion. Such configurations are generally nonbiological; however, recent studies have shown that a redox-active ruthenium(II)−phenanthroline complex (Ru^{2+}-phen) is particularly efficient at quenching the photoluminescence (PL) of QDs, and this mechanism demonstrates good potential for application as a generalized biosensing detection modality since it is aqueous compatible. Multiple possibilities for charge transfer and/or energy transfer mechanisms exist within this type of assembly, and there is currently a limited understanding of the underlying photophysical processes in such biocomposite systems where nanomaterials are directly interfaced with biomolecules such as proteins. Here, we utilize redox reactions, steady-state absorption, PL spectroscopy, time-resolved PL spectroscopy, and femtosecond transient absorption spectroscopy (FSTA) to investigate PL quenching in biological assemblies of CdSe/ZnS QDs formed with peptide-linked Ru^{2+}-phen. The results reveal that QD quenching requires the Ru^{2+} oxidation state and is not consistent with Förster resonance energy transfer, strongly supporting a charge transfer mechanism. Further, two colors of CdSe/ZnS core/shell QDs with similar macroscopic optical properties were found to have very different rates of charge transfer quenching, by Ru^{2+}-phen with the key difference between them appearing to be the thickness of their ZnS outer shell. The effect of shell thickness was found to be larger than the effect of increasing distance between the QD and Ru^{2+}-phen when using peptides of increasing persistence length. FSTA and time-resolved upconversion PL results further show that exciton quenching is a rather slow process consistent with other QD conjugate materials that undergo hole transfer. An improved understanding of the QD−Ru^{2+}-phen system can allow for the design of more sophisticated charge-transfer-based biosensors using QD platforms.

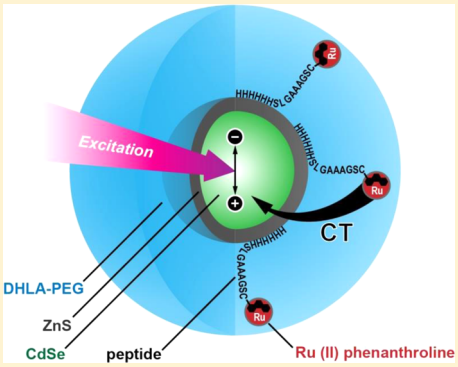

1. INTRODUCTION

Interest in exploiting nanocrystalline semiconductor quantum dots (QDs) for a wide variety of disparate applications continues to grow nearly unabated.[1−3] This interest arises primarily from the unique photophysical properties of QDs: high quantum yields; good photostability and resistance to chemical degradation; large one- and two-photon absorption coefficients across a broad range of wavelengths; and narrow photoluminescence (PL) that can be tuned as a function of both semiconductor material and core size.[4,5] These properties have already found extensive use in optoelectronic research, such as for solar energy conversion,[6] and as biological probes for imaging or sensing.[7,8] Considering the latter, QDs have been shown to be particularly useful for designing a variety of active biosensing assemblies that rely on changes in energy transfer rates as the mechanism of signal transduction.[8−11] The most prominent and successful of these configurations are based on Förster resonance energy transfer (FRET).[9−11] Here, the QD is paired with a suitable donor (D) or acceptor (A), and the proximity needed for FRET is achieved through a biomolecular linkage such as a protein, peptide, or oligonucleotide. Transduction of biological processes such as binding events or enzyme-catalyzed hydrolysis exploits D−A association or dissociation as mediated by the responsive biomolecular linkage located between the D and A. The process of FRET with QDs is sufficiently understood that on/off sensing schemes can be designed for many biological processes or analytes of interest.[8] As a consequence, other QD energy

Received: January 29, 2014
Revised: March 31, 2014
Published: April 22, 2014

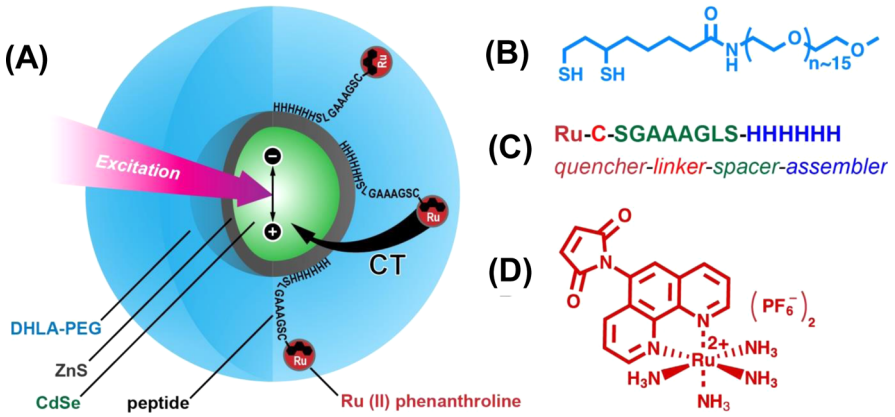

Figure 1. (A) Illustration of the CdSe/ZnS QD and Ru^{2+}-phen-labeled peptide conjugates; (B) DHLA-PEG ligand solubilizing the QDs; (C) modular design of peptide sequence; and (D) structure of Ru^{2+}-phen maleimide used to label the peptide linker.

transfer mechanisms are only partially characterized and remain underutilized, although they may also have much to offer for biosensing.[7,8,11]

In contrast to many organic fluorophores, QDs have significant surface area and, due to their reversible redox properties, are very sensitive to charge transfer processes with surface adsorbates.[12,13] Recent research has focused on harnessing charge transfer quenching of QDs for biosensing in a capacity similar to FRET.[14−21] Charge transfer is thought to offer several advantages over FRET: a putative exponential dependence on D−A separation (cf. inverse sixth power for FRET);[22] no requirement for underlying spectral overlap;[22] and potentially greater sensitivity to the medium between D and A. Consequently, the charge transfer interactions between QDs and a variety of redox-active molecules, such as catechols, are being actively studied in different biosensing formats.[15,16,23−26] Redox-active metal complexes are also particularly promising as charge transfer partners for QDs as they display many attributes that can benefit this role: well-understood redox properties that are extensively documented in the literature, including tuning of those properties through coordinating ligands, and established synthetic chemistry that uses commercially available precursors, offers high yields, and can include appended reactive chemical "handles" for labeling biomolecules.[27] Although various complexes of iridium, rhenium, osmium, and iron are commonly used in such roles, it is a ruthenium(II)−phenanthroline (Ru^{2+}-phen; see Figure 1D) that has thus far found extensive use as a charge transfer quencher for QDs in biosensing applications.[15,28]

To develop charge-transfer-based QD biosensors, the Benson group began by site-specifically labeling intestinal fatty acid binding protein, maltose-binding protein, a designer Pb^{2+}-binding protein, and a thrombin-binding DNA aptamer with Ru^{2+}-phen. These labeled proteins were then conjugated to QDs, and extensive experimental investigation with appropriate target molecules demonstrated that they could be effective charge transfer sensors for fatty acids, maltose, lead, and thrombin, respectively.[17−21] Within these composite Ru^{2+}-phen−QD assemblies, it was postulated that concentration-dependent analyte binding in the sensor complex induced structural rearrangements that altered the Ru^{2+}-phen position relative to the QD or, in the special case of the fatty acid binding protein, changes in the solvation environment. In turn, these effects resulted in a change in the rate of charge transfer between the QD and Ru^{2+}-phen and thus the QD PL intensity.

Similarly, initial work from our group has demonstrated that the rate of charge transfer quenching of QD PL depends on the number of Ru^{2+}-phen bound in proximity to the QD.[15] This result formed the basis for a protease sensor that signaled the hydrolysis of peptide linkages between the QD and Ru^{2+}-phen using the recovery of QD PL.[15] Subsequent work demonstrated that the assembly of Ru^{2+}-phen-labeled peptides to eight different colors (i.e., sizes) of QD could create a dense, spectral-multiplexing system across the visible spectrum—something that would not be possible with a single so-called dark quenching acceptor and reliance on FRET.[14] All of these studies serve to highlight the strong potential that QD−Ru^{2+}-phen interactions have for developing new types of biosensors; however, this proof-of-concept work is primarily empirical, and a detailed understanding of charge transfer quenching mechanisms in these complex QD−biomolecular−nanocrystal composite materials still remains to be achieved. As such, QD biosensors based on charge transfer quenching are currently designed without the predictive and rational design capabilities associated with FRET-based configurations.

In this work, we evaluate the underlying electrochemistry and excited state dynamics between aqueous CdSe/ZnS core−shell QDs and Ru^{2+}-phen coupled through a peptide linker (see Figure 1). A previous study of this configuration was limited to characterizing the quenching of QD PL intensity and changes in the PL excited state lifetimes on the nanosecond time scale.[15] Although useful for demonstrating the overall effect of assembling Ru^{2+}-phen with QDs, these experiments offered limited mechanistic insight. While ultrafast spectroscopy techniques have been used in more detailed physical studies of charge transfer with QDs,[23,24,26,29−33] these prior studies have been primarily nonbiological in nature, emphasizing energy conversion instead of sensing applications. In these instances, the redox active moiety has almost always been physisorbed directly to the surface of a core-only, ligand-coated QD, more oftentimes in organic rather than aqueous solvent. To gain further insight into a biologically relevant configuration, we used femtosecond transient absorption spectroscopy (FSTA) with steady-state and time-resolved PL spectroscopy to study the aqueous charge transfer quenching of core/shell QDs by peptide-linked Ru^{2+}-phen. In particular, we examine the charge carrier dynamics and directionality that lead to the quenching of QD PL when Ru^{2+}-phen-labeled peptide is assembled to the QD. Overall, we find that QD quenching requires the Ru^{2+} oxidation state, consistent with a charge

dx.doi.org/10.1021/jp501039w | J. Phys. Chem. C 2014, 118, 9239−9250

transfer mechanism, and that shell thickness around the core QD is a significant determinant of quenching efficiency. The FSTA data also show that exciton quenching is a rather slow process, consistent with other QD conjugate materials that undergo hole transfer.

2. EXPERIMENTAL SECTION

2.1. Reagents. CdSe/ZnS core−shell QDs with peak PL at 550 and 580 nm (QD550 and QD580) were synthesized as described previously[34,35] and made water-soluble with a poly(ethylene glycol) (PEG; MW ∼750 Da) appended derivative of dihydrolipoic acid (DHLA) terminating in a methoxyl group (DHLA-PEG, see Figure 1B).[36] A maleimide derivative of ruthenium(II)−phenanthroline (Ru^{2+}-phen) was synthesized as described previously.[28] All experiments were done in phosphate-buffered saline (PBS; 10 mM phosphate, 137 mM NaCl, 3 mM KCl, pH 7.4).

2.2. Peptide Labeling. The peptides used in this study are listed in Table 1 and were synthesized using standard in situ neutralization cycles with Boc-solid-phase peptide synthesis (Boc-SPPS).[37,38] Peptides were labeled with Ru^{2+}-phen maleimide, purified, desalted, quantitated, and lyophilized for storage following a protocol described in detail elsewhere.[15,39] Briefly, ca. 1 mg of peptide was dissolved in 1 mL of PBS and mixed with ca. 2−3 mg of Ru^{2+}-phen maleimide. The reaction was agitated for 2−3 h at 22−25 °C, then overnight at 4 °C. Labeled peptide was purified over nickel(II)-nitrilotriacetic acid (Ni^{2+}-NTA)-agarose (Qiagen, Valencia, CA) and desalted using a reverse-phase oligonucleotide purification cartridge (OPC; Applied Biosystems) with triethylamine acetate buffer. Purified peptide was quantitated by UV−visible absorption spectrophotometery (ε_{490nm} = 5000 M^{-1} cm^{-1} for Ru^{2+}-phen), aliquoted, dried in vacuo, and stored at −20 °C until needed.

Table 1. Ru-phen-Labeled Peptide Sequences

name	sequence[a]
P1(Ru^{2+})	(Ru^{2+}-phen)-CSGAAAGLSHHHHHH
Pro_n(Ru^{2+})	(Ru^{2+}-phen)-C$(Pro)_n$GGHHHHHH
Aib_n(Ru^{2+})	(Ru^{2+}-phen)-C$(Aib)_n$GGHHHHHH

[a]Written N- to C-terminal. See Table 3 for *n* values used.

2.3. Preparation of Ru^{3+}-phen-Labeled Peptides. Ceric ammonium nitrate, $(NH_4)_2Ce(NO_3)_6$, was dissolved in water to 100 mM. Approximately 15 μL of this solution (15 μmol) was added to a 300 μL solution of 100 μM P1(Ru^{2+}) (30 nmol) in water. The solution quickly changed from red/brown to colorless, indicating conversion to P1(Ru^{3+}). The solution was left at room temperature for 10 min before adding 300 μL of 200 mM phosphate buffer (60 μmol phosphate), upon which the solution became cloudy. This mixture was centrifuged at 5000 rcf for 2 min to give a yellow-brown pellet. The supernatant was collected, centrifuged again, and recollected. The precipitate consisted of a mixture of highly insoluble $CePO_4$ and $Ce_3(PO_4)_4$, which have pK_{sp} values >25.[40−42] Thus, addition of phosphate was a convenient means to remove to the Ce^{4+} from the peptide solution to avoid its potential oxidative effects upon peptide assembly with the QDs. While ceric ammonium nitrate is known to oxidize tryptophan and tyrosine,[43] these residues were absent from the peptides in Table 1, and thus no modifications of the remaining amino acid residues were expected. Gel electrophoresis was used to confirm that the P1(Ru^{3+}) still self-assembled to the QDs (data not shown). QD conjugates with P1(Ru^{3+}) were prepared as described below for P1(Ru^{2+}).

2.4. Ground State Absorption and PL Intensity Measurements. Ground state absorption measurements were made using an Agilent 8453 diode array spectrophotometer and quartz cuvette with a 1.00 cm path length. PL intensity measurements were acquired with peptide-linked QD−Ru^{2+}-phen conjugates at a concentration of 0.18 μM using a Tecan Infinite M1000 dual monochromator multifunction plate reader equipped with a xenon flash lamp (Tecan, Research Triangle Park, NC). The excitation wavelength used was 400 nm, corresponding to an absorption minimum for Ru^{2+}-phen (see Figure 2). The conjugates were prepared by mixing 18 pmol of QD550 or QD580 (unless otherwise indicated) with the desired equivalents of Ru^{2+}-phen-labeled peptide in 100 μL of PBS and allowing the mixture to stand in a 1.5 mL microcentrifuge tube at room temperature for 1 h prior to aliquoting into a microtiter well plate (or cuvette) for spectroscopic measurement.

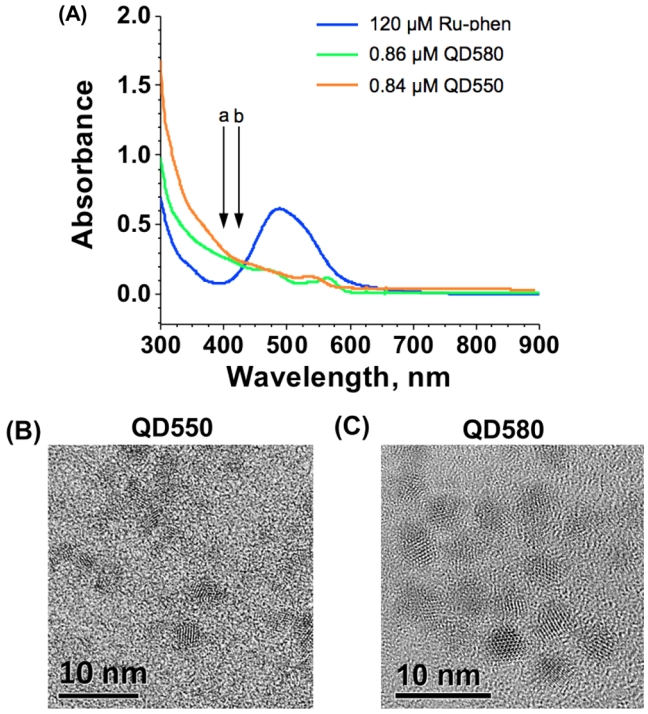

Figure 2. (A) Comparative absorption spectra for QD550, QD580, and P1(Ru-phen) measured at the concentrations indicated. (a) Excitation wavelength (400 nm) for PL intensity measurements and (b) pump wavelength (420 nm) for FSTA measurements. Representative TEM micrographs of (B) QD550 and (C) QD580 samples.

2.5. Calculation of Quenching Rates from PL Intensity Measurements. Plots of quenching efficiency, *E*, versus the average number of Ru^{2+}-phen peptides per QD, *N*, were fit with eq 1 using proFit ver. 6.2.7 (Quantum Soft, Uetikon am See, Switzerland) to determine the quenching rate constant, k_q, where *i* is the actual number of Ru^{2+}-phen-labeled peptides per QD and τ_0 the unquenched PL lifetime of the QDs. Equation 1 accounts for the Poisson distribution of peptides assembled to the QDs.[44]

dx.doi.org/10.1021/jp501039w | J. Phys. Chem. C 2014, 118, 9239−9250

$$E(N) = \sum_{i=0}^{50} \left(\frac{N^i e^{-N}}{i!} \right) \frac{ik_q\tau_0}{ik_q\tau_0 + 1} \quad (1)$$

2.6. PL Lifetime Measurements. QD PL decays were fit with a biexponential function, eq 2, and the amplitude-weighted lifetime calculated using eq 3.[45,46]

$$I(t) = A_1 \exp(-t/\tau_1) + A_2 \exp(-t/\tau_2) \quad (2)$$

$$\tau_0 = \frac{A_1\tau_1 + A_2\tau_2}{A_1 + A_2} \quad (3)$$

2.7. FSTA Spectroscopy Experiments. FSTA spectroscopy measurements of QD550 and QD580 were done using photoexcitation at 420 nm in a manner similar to that described previously.[45,46] QDs (0.5−2.0 μM) were mixed with 40 equivalents of P1(Ru^{2+}) in PBS. Control samples included solutions with only QD550 or only QD580 (0.5−2.0 μM) and solutions with only P1(Ru^{2+}) (500 μM). Experiments with lower concentrations of P1(Ru^{2+}) had poor signal-to-noise ratios, particularly in the red region of the spectrum. Samples for FSTA were prepared fresh each day, and the data are an average of three replicates. Some analysis was done using single value decomposition (SVD) with global fitting using Ultrafast Systems LLC software.

The FSTA Instruments were based on a commercial amplified Ti:sapphire laser system (1.7 kHz; Spectra-Physics Mira Oscillator and Spitfire Pro Amplifier) housed at the Center for Nanoscale Materials at Argonne National Laboratory or at the Center for Functional Nanomaterials at Brookhaven National Laboratory. A small amount of the amplifier output was used to generate the white light continuum probe, and the remaining 95% went through an optical parametric amplifier (OPA) to produce 420 nm excitation pulses at 0.7 μJ/pulse. The data were collected through a Helios spectrometer (Ultrafast Systems). The probe was delayed relative to the pump on a mechanical delay line, and the pump beam was chopped at half the repetition rate of the laser so that the absorption change (ΔA) could be measured as a function of delay time, where $\Delta A = -\log(I_{pump+probe}/I_{probe})$. The data were chirp-corrected using a solvent blank to within 100 fs over the spectral acquisition range (440−770 nm). The samples were placed in a 2 mm quartz cuvette and stirred during the acquisition. The widths of the pump and probe pulses were ca. 120 fs. The transient absorption changes at a particular probe wavelength, as a function of time, were analyzed by fitting the kinetics with a multiexponential model convoluted with a Gaussian instrument response function having a 200 fs full-width-at-half-maximum (fwhm).

2.8. Fluorescence Upconversion. QD PL quenching on the subnanosecond-to-nanosecond time scale was also confirmed using time-resolved PL upconversion (uPL) experiments at the ultrafast laser user facility at the Center for Functional Nanomaterials at Brookhaven National Laboratory. Conditions for analyzing the QD580 with Ru include a 420 nm pump, 0.6 μJ/pulse in 1x PBS with emission detected at 565 nm.

2.9. Simulating QD−Peptide Structures. Model peptides with the same sequences as $Pro_n(Ru^{2+})$ and $Aib_n(Ru^{2+})$ were constructed using the structure building tools in UCSF Chimera version 1.4.1.[47] For the polyproline peptides (n = 0, 3, 6, 12, or 18), the peptide models were constructed based on previous work.[48] For the poly(2-aminoisobutyric acid) (Aib) peptides (n = 0, 3, 6, or 9), a similar approach was taken starting with the coordinates of available Aib_n structures in the Protein Data Bank (www.rcsb.org). Energy minimization was carried out in Chimera using built-in features including ANTECHAMBER version 1.27 and the AM1-BCC method of calculating charges.[49] The polyproline helix was folded into a type II helix with φ/ψ angles of −75°/150°.[50] The Aib_n helix was folded into a 3_{10} helix with φ/ψ angles of −49°/−26°. Some representative structures derived during this modeling process are shown in the Supporting Information (SI).

3. RESULTS

3.1. QD PL Quenching. Figure 2 shows the ground state absorption spectra of QD550 and QD580, which have first exciton peaks (corresponding to band edge transitions) at 530 and 562 nm, respectively, and P1(Ru^{2+}), which has an absorption maximum at ∼490 nm. The Ru^{2+}-phen complex has only a very small absorption cross-section as compared to the QDs, and the significant differences in concentration between Ru^{2+}-phen and QD species utilized in Figure 2A amply illustrate this difference (i.e., the Ru^{2+}-phen is ∼140 times more concentrated than QD in that plot). On average, the QD550 has a 4.5 ± 0.7 nm diameter (2.5 nm diameter CdSe core and a 1.0 nm thick ZnS shell), while the QD580 has a 4.8 ± 0.8 nm diameter (3.3 nm diameter CdSe core and a 0.7 nm thick ZnS shell), as extrapolated from the synthetic conditions and TEM micrographs (average of >100 QDs with standard deviations of ±15%; see Figure 2). Figure 3 shows PL emission spectra for the QD550 and QD580, highlighting a progressive quenching response as the number of assembled P1(Ru^{2+}) per QD increases. The QD−P1(Ru^{2+}) conjugates were excited at 400 nm, which minimized optical excitation of the Ru^{2+}-phen. Interestingly, these two QD materials exhibited different trends in their quenching, with the QD580 being quenched more strongly than the QD550. The data in Figure 3 were fit to eq 1 to determine the relative quenching rates, $k_q\tau_0$. Measurement of the QD PL lifetimes then permitted extraction of the quenching rate constants, k_q. The QD550 and QD580 PL decays (data not shown) were fit with a biexponential decay, and the amplitude-weighted average lifetime was taken as τ_0. The QD PL decay constants and the quenching rate constant for P1(Ru^{2+}) are listed in Table 2 for each of the native QD samples. The P1(Ru^{2+}) quenches the QD580 ca. 20-fold more efficiently than QD550, with a rate comparable to the intrinsic excited state decay rate of the QD580 (1.1×10^8 s^{-1}). Although much slower charge transfer quenching was observed with the QD550, its intrinsic decay rate (8.6×10^7 s^{-1}) was similar to that of the QD580, and the degree of this quenching can be seen in Figure 3B. The latter value is suggested to be dominated by the QD's much slower and less prominent lifetime component in a complex manner.

Similar to our initial findings,[15] analysis of the PL spectra revealed that both QD550 and QD580 exhibited PL quenching that was independent of the emission wavelength (see SI, Figure S1). The QD580 (full width at half-maximum, fwhm = 32 nm) exhibited only a <2% relative standard deviation (RSD) in wavelength-dependent quenching efficiency within ±30 nm of the peak PL. The QD550 (fwhm = 27 nm) exhibited a slightly larger RSD of ca. 10%; however, this can be attributed to the effect of instrumental noise in conjunction with the lower overall quenching efficiencies compared to the QD580. Importantly, the slopes of the lines of best fit for the

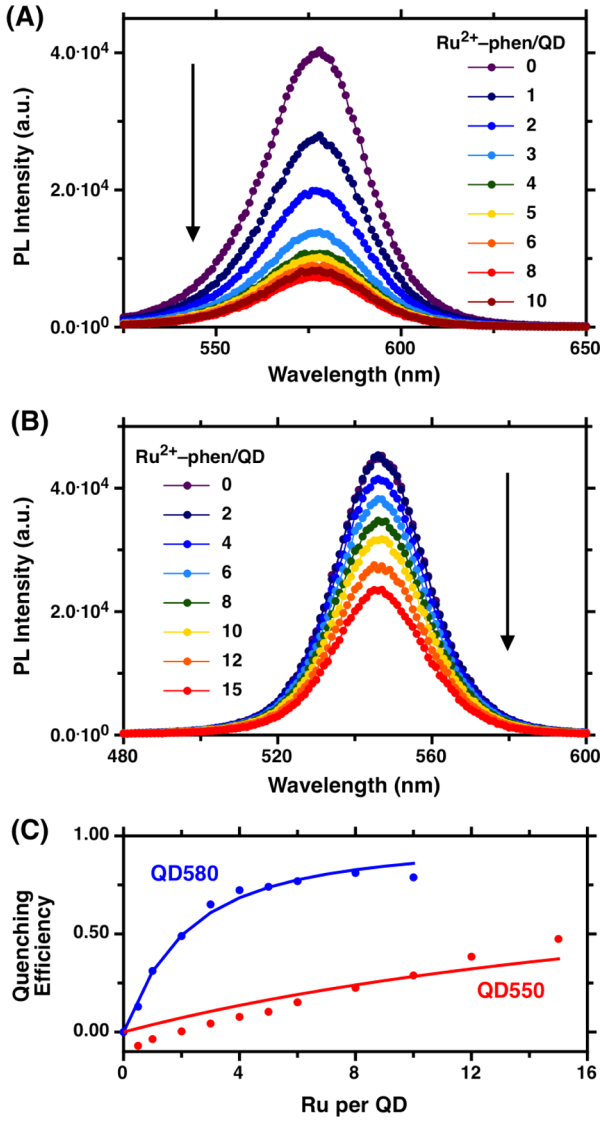

Figure 3. Quenching of (A) QD580 and (B) QD550 PL as a function of the assembly of increasing amounts of P1(Ru^{2+}) per QD, photoexcited at 400 nm. (C) Quenching efficiency as a function of the average number of P1(Ru^{2+}) per QD. The slightly negative quenching efficiencies at low numbers of P1(Ru^{2+}) per QD550 are due to a small increase in the QD quantum yield as peptide is assembled before quenching by the Ru^{2+}-phen becomes significant. This phenomenon is often seen with the assembly of proteins onto the QD surface and is believed to arise from surface passivation effects.[77]

Table 2. QD PL Decay Constants and Quenching Rate Constant

	τ_0 (ns)	A_1	τ_1 (ns)	A_2	τ_2 (ns)	$k_q\tau_0$	k_q (s^{-1})
QD550	11.7	73%	14.8	27%	3.3	0.045	3.8×10^6
QD580	9.0	63%	12.2	37%	3.4	0.68	7.6×10^7

wavelength-dependent quenching efficiencies were insignificant: 0.03 ± 0.01% and 0.03 ± 0.04% for the QD580 and QD550, respectively. Wavelength-dependent QD quenching would provide evidence of underlying spectral overlap with a proximal acceptor, and this, in turn, would be indicative of FRET-based energy transfer processes.[15,45,46,51]

3.2. Comparing QD Quenching Between Ru^{2+}-phen and Ru^{3+}-phen. We next investigated quenching of QD PL with the assembly of P1(Ru^{3+}). This would help confirm whether the Ru center was acting as an electron donor or acceptor by chemically changing its ability to perform this function. This, in turn, could also provide evidence for the directionality of charge transfer. Conversion of the P1(Ru^{2+}) to P1(Ru^{3+}) via oxidation with Ce^{4+}(aq) was confirmed by loss of the visible absorption band associated with Ru^{2+}-phen, as shown in Figure 4A. Upon assembly of P1(Ru^{3+}) with QD580,

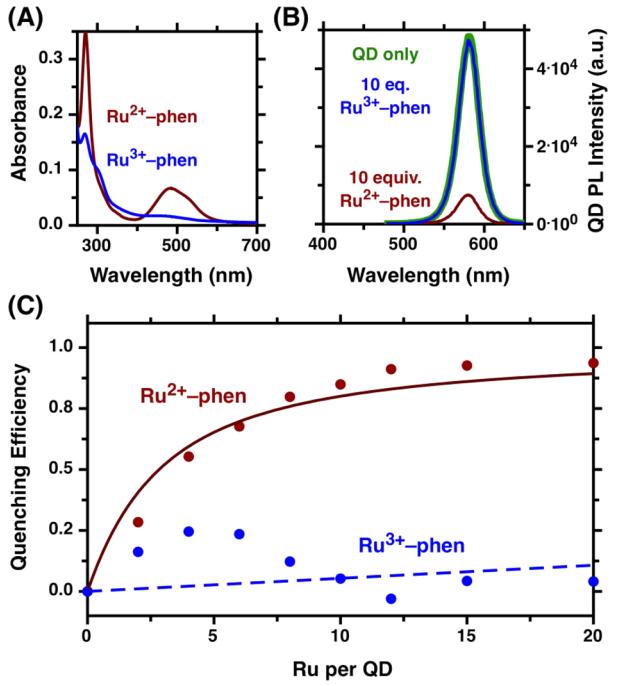

Figure 4. (A) Ground state absorption spectra of Ru^{2+}-phen and Ru^{3+}-phen (obtained from the oxidation of the Ru-phen with Ce^{4+}). (B) Quenching of QD580 PL with and without ~10 equiv of Ru^{2+}-phen or Ru^{3+}-phen. (C) Quenching efficiency as a function of the number of Ru^{2+}-phen- or Ru^{3+}-phen-labeled peptides assembled per QD580. The latter does not effectively quench the QD PL.

little or no quenching of PL was observed (Figure 4B,C). A parallel control experiment with the assembly of equivalent amounts of Ru^{2+}-phen again showed strong quenching (k_q = 4.9 × 10^7 s^{-1}; the small discrepancy with the value in Table 2 is attributed to a different batch of DHLA-PEG coating, as discussed later).

3.3. Effect of Changing the Peptide Linker Length. In a final set of steady-state quenching experiments, we investigated the effect of peptide length on the charge transfer quenching rate constant. Polyproline (Pro_n) and poly(2-aminoisobutyric acid) (Aib_n) peptides were used for this purpose and assembled with QD580 at average ratios varying from 0 to 18. The quenching rate constants are listed in Table 3. The quenching rate peaked at n = 3 for both the Pro_n(Ru^{2+}) and Aib_n(Ru^{2+}) and generally decreased for higher values of n. However, the quenching rate did not exhibit an exponential decrease as the peptide length increased, as might be expected a priori.

3.4. FSTA Experiments. Transient absorption (TA) measurements of QD550, QD580, and their P1(Ru^{2+}) conjugates are summarized in Table 4 and Figure 5. The TA spectra of the QD550 and QD580 showed similar ground state

dx.doi.org/10.1021/jp501039w | J. Phys. Chem. C 2014, 118, 9239–9250

Table 3. Quenching Rate Constants for $(Pro)_n(Ru^{2+})$ and $(Aib)_n(Ru^{2+})$

peptide	helix length (Å)	QD−Ru separation[a]	$k_q\tau_0$	k_q (s^{-1})	uncertainty[c]
Pro_0	0.0	25.4	0.86	9.5×10^7	±6%
Pro_3	8.6	35.6	1.1	12×10^7	±9%
Pro_6	17.7	37.4	0.63	7.0×10^7	±17%
Pro_{12}	29.7	65.1	0.65	7.2×10^7	±6%
Pro_{18}	54.1	71.6	0.44	4.9×10^7	±8%
Aib_0	0.0	25.4	0.64	7.2×10^7	±18%
Aib_3	5.6	29.5	0.84	9.4×10^7	±8%
Aib_6	12.3	33.7	0.44	4.9×10^7	±13%
$Aib_{9(AVG)}$[b]	18.7	37.7	0.25	2.8×10^7	±26%
$Aib_{9(MIN)}$[b]	18.7	29.9	0.25	2.8×10^7	±26%
$Aib_{9(MAX)}$[b]	18.7	45.5	0.25	2.8×10^7	±26%

[a]QD surface to Ru center estimated from structural modeling as described in the Experimental Section. [b]The data for Aib_9 are poorly fit by eq 1, thus approximate minimum, maximum, and average distances for the QD−Ru^{2+}-phen separation were also considered. [c]Estimated uncertainty based on fitting of quenching data with eq 1. Fits are in SI.

recovery kinetics with nearly 30−40% of the initial excited state population decaying biexponentially within 100 ps. The remaining 60−70% of the decay was a long-lived component with an average lifetime of 6 ns, which approached the longest lifetime that could be measured by the TA systems. Interestingly, the amplitude-weighted excited state lifetimes for the QD550 and QD580 were indistinguishable, and the differences between the individual decay components were within the uncertainty of the experiment. Furthermore, the lifetimes of the ground state bleach were wavelength dependent. A similar observation was made by Burda et al. with CdSe QDs, who suggested that this feature could be indicative of dark excited states.[29] With the addition of an average of 40 $P1(Ru^{2+})$ per QD, the TA signature for the QD ground state recovery changed moderately, with a decrease in the amplitude-weighted excited state lifetime to ca. 2.6−2.7 ns for both the QD550 and QD580. Forty equivalents of $P1(Ru^{2+})$ were used to ensure saturation of the charge transfer quenching effect with both QDs. No changes in the Ru^{2+}-phen TA spectrum could be unambiguously detected because the Ru^{2+}-phen was very weakly absorbing, even when used at relatively high ratios/concentrations.

4. DISCUSSION

4.1. Peptide Design and Assembly to QDs. A key feature of this study was having the Ru^{2+}-phen moiety coupled to a peptide linker which, in turn, could be reliably and controllably self-assembled to the QDs. The P1 peptide sequence, C·SGAAAGLS·HHHHHH, is shown as divided into three functional modules: the N-terminal cysteine residue provided a unique thiol group for labeling with Ru-phen maleimide and acts as the linker between these disparate entities; the intermediate SGAAAGLS sequence functioned as a spacer that was able to pivot on the flexible GLS portion; and the C-terminal hexahistidine (His_6) assembled and anchored the peptide to the QD (Figure 1). His_6-appended peptides, proteins, and even oligonucleotides can self-assemble, via

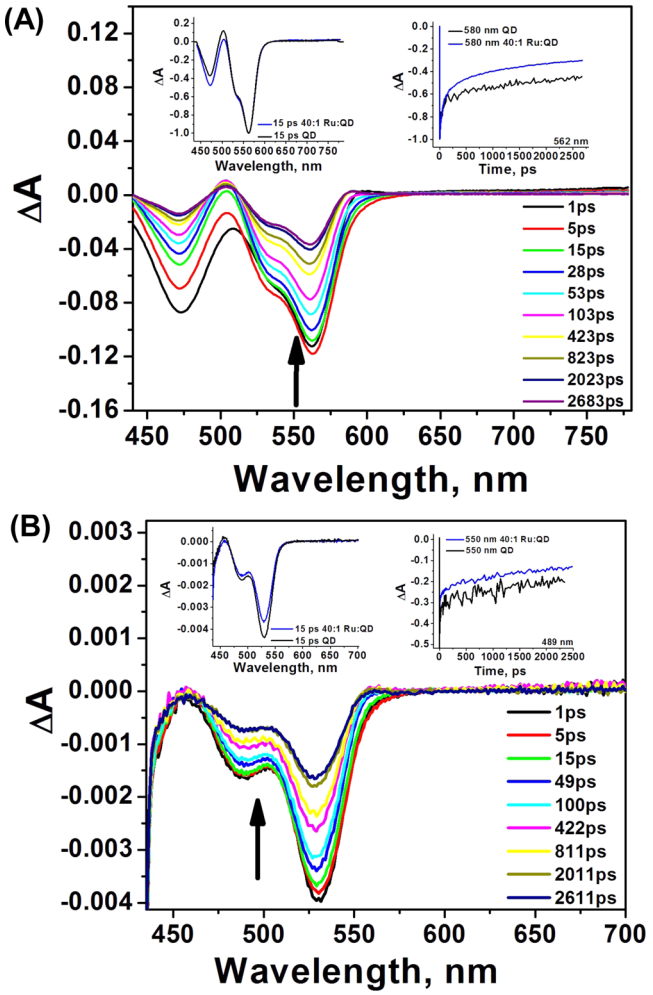

Figure 5. (A) TA spectra of 40:1 Ru-phen-pep:QD550 in PBS buffer, photoexcited at 420 nm. The inset on the left is the 15 ps spectrum versus QD alone. The inset on the right is the ground state recovery trace monitored at 489 nm. (B) TA spectra of 40:1 Ru-phen-pep:QD580 nm in PBS buffer, photoexcited at 420 nm. The inset on the left is the 15 ps spectrum versus QD alone. The inset on the right is the ground state recovery trace monitored at 562 nm.

Table 4. Kinetic Fits of QD and QD−$P1(Ru^{2+})$ Transient Absorption Components[a]

system	A_1 (%)	τ_1 (ps)	A_2 (%)	τ_2 (ps)	A_3 (%)	τ_3 (ns)
QD550	17.2 ± 10.0	13.4 ± 8.0	14.6 ± 6.5	91 ± 44	68.2 ± 5.0	5.9 ± 0.6
QD550−$P1(Ru^{2+})_{40}$	5.6 ± 1.0	<0.250	24.8 ± 5.3	60 ± 17	69.6 ± 5.3	3.8 ± 0.3
QD580	22.3 ± 8.4	16.2 ± 3.2	16.2 ± 3.2	100 ± 14	61.5 ± 5.5	6.7 ± 0.6
QD580−$P1(Ru^{2+})_{40}$	35.0 ± 8.7	33.0 ± 13.2	24.0 ± 4.0	306 ± 80	41.0 ± 7.2	6.6 ± 0.6

[a]Kinetic fits are a sum of exponentials with a Gaussian 250 fs instrument response function and based on the standard use of $\Delta A(t)$ = IRF + $(\Sigma_i^3 A_i e^{-k_i t})$. Data are an average of five kinetic analyses over the range from 520 to 560 nm, and the percentage of each amplitude component is indicated by A_n (%).

dx.doi.org/10.1021/jp501039w | J. Phys. Chem. C 2014, 118, 9239−9250

spontaneous metal-affinity coordination, to the ZnS surface of CdSe/ZnS QDs functionalized with a variety of coatings.[37,52−54] The binding interaction is characterized by rapid assembly (seconds to minutes), a high affinity equilibrium binding constant ($K_a \sim 1 \times 10^9$ M^{-1}), control over the number of biomolecules assembled per QD (i.e., conjugate valence) on the basis of stoichiometry, and at least some control over their orientation.[37,52−54] Here, the His_6 sequence binds to the QD surface, while the GLS can adopt a conformation that extends the rest of the peptide sequence away from the QD surface and into the surrounding layer of PEG ligands. The His_6 also provided another critical function in that it allowed for facile purification of labeled peptide using immobilized metal-affinity chromatography (IMAC).[39] The other peptides used in this study were the helix-forming Pro_n and Aib_n sequences,[55,56] which offer some ability to incrementally control the distance between the QD and Ru^{2+}-phen. This arises as the helices for both motifs are predicted to be quite rigid and should minimize bending of the peptide toward the QD surface. Furthermore, the use of a bulky PEGylated surface ligand will also contribute in a steric manner toward directing the peptides away from the QD surface. Indeed, this rationale has been used before successfully with QD−peptide bioconjugates.[48] It is important to note, however, that this still does not completely preclude some peptides assuming bent or otherwise altered conformations which could affect charge transfer. As shown in Figure 1A, the conjugation of the Ru^{2+}-phen to the QDs using the His_6-terminated peptide is expected to result in a centrosymmetric arrangement or display of the Ru-phen around the QD (albeit that the peptide should have some conformational freedom).[57] Comparison of this peptide to similar sequences used in a prior FRET study suggests that the P1 peptide assembly places the Ru^{2+}-phen ca. 34−37 Å from the QD surface.[57] The distance is within the linear extension of the DHLA-PEG ligands on the surface the QD. Previous work has also shown that QDs of similar size, and functionalized with DHLA-based ligands, can display a maximum of ca. 50 ± 10 His_6-terminated peptides.[58] Here, we use an average of ≤40 peptides per QD, which, although slightly below saturation, is still sufficient to elicit a significant QD quenching response.

It is also important to note that the Ru atom interaction with the phenanthroline moiety is considered a coordination metal complex with coordinate covalent bonds. The coordinate covalent bond is a chemical bond in which both bonding electrons are from the ligand, and such phenanthroline complexes are considered very stable.[27] Our initial work also demonstrated that the free Ru-phen complex has a very small direct interaction with the PEGylated QDs utilized here due to electrostatic interactions,[15] and this interaction could be counteracted by the presence of NaCl in PBS as done here. From a practical standpoint this means that, at the experimental concentrations utilized here, the Ru-phen complex does not significantly contribute to QD quenching via direct physical interactions with the QD surface, nor will the Ru atom dissociate from the phenathroline complex which cumulatively alleviated our concerns about these issues.[15,27]

4.2. Energy Levels of Ru^{2+}-phen and QDs. We have previously measured the cyclic voltammograms of CdSe/ZnS QDs coated with DHLA-PEG ligands and found a broad, irreversible oxidation peak at E^0_{ox} = 0.22 ± 0.2 V (vs Ag/AgCl).[15] A prior estimate also places the conduction band and valence band edges of the QDs between −1.1 to −1.2 V and 0.8 to 0.9 V (vs Ag/AgCl), respectively.[15] A cyclic voltammogram for the Ru^{2+}-phen is shown in the SI (Figure S5) and exhibited two broad irreversible reduction peaks with cathodic peak potentials (E_{pc}) centered at −1.16 and −1.33 V (vs Ag/AgCl), as well as the reversible Ru^{2+}/Ru^{3+}redox couple at $E_{1/2}$ = 314 mV (vs Ag/AgCl). This half-wave potential is intermediate to the expected conduction and valence band edges of the QDs and slightly higher in energy than the oxidation level(s) of the QDs. This alignment is, a priori, favorable for hole transfer from the QD to the Ru^{2+}-phen. In our previous study, the peptide-linked assembly of metal complexes with oxidation potentials intermediate to the expected band edges, but also lower in energy than the oxidation levels of the QD (e.g., ferrocene), did not cause quenching of QD PL.[15] These oxidation states, which are thought to correspond to surface states, are critical for charge transfer quenching.

4.3. Quenching Efficiencies. The quenching of QD PL via Ru^{2+}-phen-labeled peptides has been previously attributed to electron transfer from the Ru^{2+} to the QD with the suggestion of concomitant hole transfer from the QD.[15] This mechanism of charge transfer was inferred from ground state absorption spectra and consideration of the redox levels for the QD and Ru^{2+}-phen. In general, charge transfer quenching efficiency was observed to increase with decreasing QD size and with a greater average number of Ru^{2+}-phen per QD. Not surprisingly, surface ligand character also appeared to significantly influence the quenching behavior as well.[15,59] Here, we again observed that quenching efficiency increased as the number of proximal Ru^{2+}-phen displayed around the QD increased. However, we also observed that two QDs of similar size (4.5 ± 0.7 nm diameter for core/shell QD550 and 4.8 ± 0.8 nm for QD580) and modified with the same surface ligands can manifest vastly different quenching efficiencies: CdSe/ZnS QD580 had a quenching rate constant of $k_q \sim 8 \times 10^7$ s^{-1}, which was an order of magnitude larger than the $k_q \sim 4 \times 10^6$ s^{-1} associated with CdSe/ZnS QD550 and the same peptide, P1(Ru^{2+}). The QDs had comparable PL lifetimes, measured as ∼9 ns (QD580) and ∼12 ns (QD550), identical quantum yields (14%), and neither exhibited any significant defect emission. The discrepancy between the QD550 and QD580 quenching efficiencies, despite their similar macroscopic PL properties, suggests that the structure of the QD interface is critically important in determining charge-transfer-based quenching efficiency. One such difference here was that the QD580 samples had a shell 0.3 nm thinner than the QD550. Given that the shell is expected to be one of the principal impediments to charge transfer between the Ru^{2+}-phen and QD core, it appears that angstrom-scale changes in shell thickness, or more uniform coverage that appears as a thicker shell, can cause significant changes in the rate of charge transfer in these samples. In support of this hypothesis, Zhu et al. have reported that the rate of electron transfer from CdSe/ZnS QDs to an adsorbed dye, in a hydrophobic system, has an exponential dependence on the shell thickness.[60]

In contrast to the putatively strong influence of ZnS shell thickness, the distance dependence of the quenching effect arising from just peptide extension alone appears to be rather modest, despite charge transfer quenching occurring over QD surface-to-Ru^{2+}-phen distances that are estimated to vary between ca. 25 and 80 Å for the Pro_0 through Pro_{18} peptides, respectively. The Aib_n series of peptides are chemically different from Pro and are expected to allow the Ru^{2+}-phen to maintain a slightly closer approach to the QD surface. However, it is important to note that through-bond charge transfer from

dx.doi.org/10.1021/jp501039w | J. Phys. Chem. C 2014, 118, 9239−9250

metal centers across peptide structures can be quite complex with the possibility of different residues providing either neutral, conductive, or insulative properties.[61] The lack of significant quenching effects versus distance with these peptides may be more reflective of their inherent properties and environment or, alternatively, may reflect the more dominant role of shell size effects on charge transfer. Although certainly worthy of future study, the effect of the peptide sequences/residues on charge transfer processes in these systems is beyond the current scope.

4.4. Evidence Against Resonance Energy Transfer. In our initial study, steady-state and time-resolved fluorescence on the nanosecond time scale was used to extensively study the quenching of QD PL with several metal complex−peptide conjugates that varied in oxidation potential including the current Ru-phen−peptides.[15] When QDs were assembled with redox active molecules that did not have favorable energy matching for charge transfer, only a minor amount of PL signal was quenched (<20%) with no change in the QD lifetime. Critically, it was shown that QD PL could only be efficiently quenched by the Ru-phen−peptide, the only complex with a favorable energy level match to the QD donor.

The results in Figure 4C, which show that Ru^{3+}-phen does not elicit any significant quenching effect when brought into proximity of the QD, unambiguously demonstrate that a Ru^{2+} center is required to quench QD PL. The HOMO electron of ground state Ru^{2+}-phen is thus integral to the quenching mechanism. This result is consistent with the previously posited mechanism for hole transfer from the QD $1S_h$ state to the Ru^{2+}-phen (i.e., electron transfer from the Ru^{2+}-phen HOMO). However, as shown in Figure 4A, the oxidative transition between Ru^{2+}-phen and Ru^{3+}-phen also changes the absorption spectrum of the complex, potentially resulting in a change in the spectral overlap integral relevant to a FRET mechanism of quenching; the latter process has recently been reported for similar QD−peptide bioconjugates labeled with Os^{2+} complexes and C_{60}.[45,46,62] In the current example, the overlap decreases from 2.2×10^{-11} and 1.4×10^{-11} cm^6 mol^{-1} for Ru^{2+}-phen with QD550 and QD580, respectively, to $<0.7 \times 10^{-11}$ cm^6 mol^{-1} for Ru^{3+}-phen with either QD. These overlaps for Ru^{2+}-phen are between 10- and 100-fold smaller than those observed for typical QD−dye FRET pairs.[63] To obtain a FRET efficiency of ∼75% with 4 P1(Ru^{2+}) per QD, the Ru^{2+}-phen would need to be located ∼3.0 nm from the center of the QD, which is not physically possible with the QD580 (core radius ∼3.3 nm from TEM, plus a 0.7 nm thick shell). Further, the quenching rate for P1(Ru^{2+}) with the QD550 should be 20% larger than with QD580; however, this was not observed, and neither QD exhibited wavelength-dependent quenching efficiency when conjugated to and quenched by the Ru^{2+}-phen, as would be expected for FRET.[46,51] Indeed, wavelength-dependent quenching can be considered a hallmark of QD quenching by FRET.[46,51] A preliminary conclusion to the same effect was also reached in our previous examination of QD−Ru^{2+}-phen interactions.[15] Given the foregoing, a FRET mechanism of quenching can be conclusively ruled out. Cumulatively, quenching appears to be through electronic interactions between Ru-phen−peptide and the linked QD, and in conjunction with the above, hole transfer from the QD to the Ru^{2+}-phen therefore becomes a more probable mechanism of quenching.

4.5. FSTA Experiments. The excited state dynamics of CdSe and CdS QDs have been previously examined under various conditions and solvents using TA spectroscopy.[13,29] Direct photoexcitation of the QD results in a ground state bleach of the 1S state and the corresponding intraband electronic transition in the visible region. The time scale of this process is on the order of hundreds of femtoseconds with a multiexponential recovery that is attributed to conduction band filling and surface trapping of charges that persist on the nanosecond to microsecond time scale.[29,64] Changes in TA spectra and dynamics can sometimes provide evidence for charge transfer. For example, electron transfer from QDs to an adsorbed viologen dye was identified through near complete bleaching of the QD's band-edge TA signal and parallel observation of a spectral signature for the reduced form of the adsorbed dye.[12] Hole transfer from QDs to adsorbates has been more difficult to identify from TA spectra, relying on spectral signatures from the oxidized adsorbate,[31,32] because the QD TA spectra reflect conduction band electron dynamics that are not involved in the initial transfer. However, a state-resolved approach has been described by Kambhampati and co-workers that resolves dynamics through selective state pumping and probing.[65] When QDs are photoexcited directly into specific states, the electron relaxation dynamics, hot exciton relaxation dynamics, and transitions from first excited states for holes and electrons can be resolved. More recently, time-resolved PL experiments in conjunction with TA have provided insight into hole dynamics indirectly. For example, Sykora et al. reported that the PL of hydrophobic CdSe QDs coated with trioctylphosphine oxide and adsorbed Ru−polypyridine complexes are quenched through hole transfer from the QD to the Ru−polypyridine complex.[26] This conclusion was arrived at through both FSTA studies of the charge carrier dynamics and time-resolved PL upconversion (uPL) experiments. The carrier dynamics were characterized by a 5 ps depopulation of the QD hole states;[26] however, the distance between the QD and adsorbed Ru−polypyridine complex was extremely small and was not varied.

Here, the confounding issue is that the TA spectra showed no features that could be unambiguously attributable to the oxidized (Ru^{3+}) or reduced (Ru^{2+}) Ru-phen complex. Despite the strong structural similarities to Ru^{2+} complexes with 2,2′-bipyridine ligands, the spectra of 1,10-phenanthroline (phen) excited ^{3}*MLCT states as *bis*- and *tris*-phen ligands have not been easily observed under normal light intensities.[66,67] The TA spectrum of the Ru^{2+}-phen-labeled peptide alone, shown in SI Figure S3, exhibits a positive transient feature between 550 and 700 nm. This absorption has a biexponential decay (τ_1 = 16 ps and τ_2 = 700 ps), where the 700 ps decay matches the monoexponential recovery of the ground state bleach at 472 nm. Comparing the TA spectra between the QD580 alone and its assembly with Ru^{2+}-phen, small spectral differences in the ground state bleach were observed, which were then analyzed by single value decomposition (SVD) with global fitting to reveal a 5 ps component that corresponded to the Ru^{2+}-phen ground state bleach at 472 nm (see Figure S4, SI). It is likely that direct photoexcitation of Ru^{2+}-phen at 420 nm leads to a minor population of ^{3}*Ru^{2+}-phen. In experiments with QDs, the Ru-phen-labeled peptide concentrations were below 100 μM, and at this concentration they would have contributed <5% of the total signal at 530 nm, a value that is essentially negligible. The TA spectrum of the QD580-P1(Ru^{2+}) assemblies showed a positive absorption feature ($\Delta A \sim 10^{-3}$) between 550 and 700 nm. The TA spectrum for the QD550-P1(Ru^{2+}), however, shows no such feature within the

dx.doi.org/10.1021/jp501039w | J. Phys. Chem. C 2014, 118, 9239−9250

experimental precision. Notwithstanding the lack of evidence for FRET in other experiments, the positive TA feature is not sufficiently pronounced to be consistent with FRET, in contrast to recent results from a previous assembly consisting of QDs paired with Os^{2+}–peptidyl complexes.[46]

Within the QD550–Ru-phen assemblies, charge transfer occurred after photoexcitation with a recovery half-life of $\tau_{1/2}$ = 1.3 ns in contrast to the $\tau_{1/2}$ = 383 ps for the QD580–Ru-phen assemblies. Interestingly, the QD580 PL was quenched more strongly than the QD550 PL and exhibited a faster recovery. The QD bleach kinetics, however, only provide insight into the dynamics of conduction band state electrons and do not reflect hole dynamics.[65] Retention of the QD bleach suggests no substantial conduction band electron dynamics occur on the ultrafast time scale. Previously, Huang et al. found that CdSe QDs with adsorbed $Re(CO)_3Cl(dcbpy)$ (dcbpy = 4,4′-dicarboxy-2,2′-bipyridine) (E^0_{red} = −1.0 vs Ag/AgCl) undergo photoinduced electron transfer from the conduction band of the CdSe QDs to the Re complex with $\tau_{1/2}$ = 2.3–1000 ps depending on core size.[32] This analysis was based on fitting the QD ground state bleach kinetics. Since the electronic absorption of the Ru^{3+}-phen was not observed in TA spectra, the lifetimes of electron transfer and ground state recovery were estimated from the kinetics of the spectral bleaching traces recorded between 520 and 560 nm for the Ru^{2+}-phen assembled to the QD550 and QD580. This region corresponded to the maximum QD bleach, with minimal contribution from the Ru^{2+}-phen ground state.

Again, we note that extensive time-resolved fluorescence data were collected in our initial report on the nanosecond time scale when a significant population of the excited state has been quenched.[15] This explains why a smaller population of quenching of the QD exciton state is observed by the femtosecond transient absorption experiments here. QD PL quenching on the subnanosecond-to-nanosecond time scale was also confirmed using time-resolved PL upconversion (uPL) experiments. Figure 6 shows a rather slow quenching process,

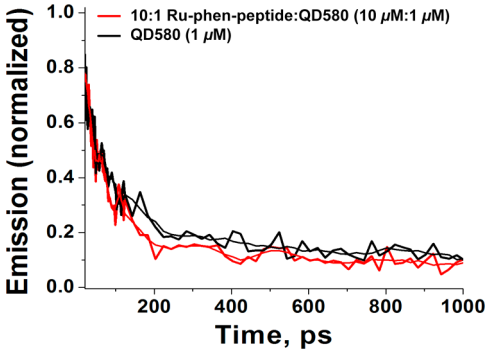

Figure 6. Femtosecond upconversion kinetics of the QD emission for 10:1 Ru-phen–peptide (10 μM):QD580 (1 μM) photoexcited at 420 nm. Data shown are the average of 4 traces. No emission was observed for Ru-phen–peptide alone.

and the rate of this quenching lies on a time scale that is not accurately measured because of the TA and uPL delay tracks. Using Figure 6, the QD PL is quenched by 43% on the 0.9–4.0 ns time scale. The results observed here are consistent with the slower dynamics expected when the distance of the QD and Ru-phen–peptide is lengthened. In contrast, the aforementioned studies by Sykora measured the charge transfer dynamics using uPL and FSTA on QDs with electrostatically adsorbed Ru–polypyridine complexes and reported a 5 ps uPL decay.[26]

5. CONCLUSIONS

In summary, we build from our previous reports demonstrating the quenching of QD PL by proximal, peptide-linked, Ru^{2+}-phen complexes.[14,15] Although a charge-transfer process was implicated, we were unable to unambiguously define the mechanism or stipulate the directionality of electron and/or hole transfer. Here, we contribute more to the understanding of QD quenching by this charge transfer process. First, we find that resonance energy transfer can be conclusively ruled out as the mechanism of quenching. Comparison of QD interactions with Ru^{2+}-phen and Ru^{3+}-phen-labeled peptides further reveals that the Ru^{2+} state is essential for QD quenching. This result provides strong indirect evidence for hole transfer from the QD to the Ru^{2+}-phen, which, importantly, is mechanistically feasible and consistent with all experiments to date.

The difference in PL quenching efficiency between QD550 and QD580, along with a comparison among Ru^{2+}-peptides of differing persistence length, suggests that shell thickness is a most critical determinant of charge transfer rates in these assemblies. This observation, in conjunction with our earlier observations that QD surface coating (i.e., negatively charged DHLA versus neutral DHLA-PEG) contributed to observable differences in Ru^{2+}-phen charge-transfer-based processes,[15] suggests that the interfacial environment of the QD strongly influences charge transfer quenching efficiency. This result is not unexpected given the growing literature describing such phenomena.[59,68−70] The QD interface, especially in an aqueous buffer, is a complex environment with the possibility of both major and subtle contributions from crystal facets, shell coverage, ligand densities, and solvation, along with other complicating factors such as localized pH gradients at the QD surface. FSTA and uPL analysis reveals that the rate of QD quenching is slow on the ultrafast time scale and occurs in the nanosecond rather than picosecond regime. This analysis is, however, complicated by the lack of an unambiguous spectroscopic signal from the Ru^{2+}-phen. Interestingly, these findings are mechanistically similar to those reported by Huang et al. for CdSe QDs interacting with an adsorbed Re compound.[32] This is also consistent with the rate of hole transfer in other QD assemblies including those described in refs 25 and 71. We do note that our system is more complicated than many others because it was constituted in the high-salt, aqueous environment typically needed for biosensing. Further experiments will focus on pairing differently functionalized QDs with Ru^{2+}-phen and other redox-active metal complexes in a similar environment to try to elucidate the contributions of the solubilizing ligands and localized environment.

A mechanistic picture of the charge transfer quenching of biologically relevant, core/shell QD bioconjugates with Ru^{2+}-phen may provide a means of creating QD probes that have improved sensitivity and greater versatility for detecting a more diverse range of biological processes and analytes or, alternatively, that respond to biochemical redox stimuli rather than biomolecular interactions.[61] Determining the direction of charge transfer and identifying the states involved remains critically important to this endeavor as it may enable the design of systems where charge transfer is "intercepted" by species in biologically relevant redox pathways, resulting in light-up

dx.doi.org/10.1021/jp501039w | J. Phys. Chem. C 2014, 118, 9239–9250

sensors that transduce, for example, cellular metabolism. The detection and visualization of redox pathways in biological systems still remains exceedingly challenging.[72,73] As noted, QDs are already well developed for fluorescent cellular and small animal labeling[74−76] and for FRET-based sensing.[8−11] When better understood, charge transfer interactions with QDs may add a new dimension to such sensing and imaging applications and open up new avenues for probing biological systems.

■ ASSOCIATED CONTENT

Supporting Information

Additional FSTA experimental data, some representative data, and supporting analysis. This material is available free of charge via the Internet at http://pubs.acs.org.

■ AUTHOR INFORMATION

Corresponding Authors

*E-mail: amscott@miami.edu

*E-mail: igor.medintz@nrl.navy.mil.

Present Address

▽Department of Chemistry, University of British Columbia, 2036 Main Mall, Vancouver, BC V6T 1Z1, Canada.

Notes

The authors declare no competing financial interest.

■ ACKNOWLEDGMENTS

The authors acknowledge NRL, the NRL NSI, Office of Naval Research, and the Defense Threat Reduction Agency. J.B.B.-C. acknowledges a Marie Curie IOF. W.R.A. is grateful to the Natural Sciences and Engineering Research Council of Canada (NSERC) for a postdoctoral fellowship. A.M.S. acknowledges the ANSER Center, an Energy Frontier Research Center funded by the U.S. Department of Energy, Office of Science, Office of Basic Energy Sciences. Molecular graphics images were produced using the UCSF Chimera package from the Resource for Biocomputing, Visualization, and Informatics at the University of California, San Francisco (supported by NIH P41 RR-01081). A.M.S. was a postdoctoral researcher at Argonne National Laboratory from 2009 to 2010, and some of the ultrafast transient absorption measurements described here were performed at the Center for Nanoscale Materials nanophotonics laser user facility.

■ REFERENCES

(1) Vivero-Escoto, J. L.; Huang, Y. T. Inorganic-Organic Hybrid Nanomaterials for Therapeutic and Diagnostic Imaging Applications. *Int. J. Mol. Sci.* **2011**, *12*, 3888−3927.

(2) Zhang, G. Q.; Finefrock, S.; Liang, D. X.; Yadav, G. G.; Yang, H. R.; Fang, H. Y.; Wu, Y. Semiconductor Nanostructure-Based Photovoltaic Solar Cells. *Nanoscale* **2011**, *3*, 2430−2443.

(3) Chandrasekaran, J.; Nithyaprakash, D.; Ajjan, K. B.; Maruthamuthu, S.; Manoharan, D.; Kumar, S. Hybrid Solar Cell Based on Blending of Organic and Inorganic Materials-An Overview. *Renewable Sustainable Energy Rev.* **2011**, *15*, 1228−1238.

(4) Zrazhevskiy, P.; Sena, M.; Gao, X. H. Designing Multifunctional Quantum Dots for Bioimaging, Detection, and Drug Delivery. *Chem. Soc. Rev.* **2010**, *39*, 4326−4354.

(5) Rosenthal, S. J.; Chang, J. C.; Kovtun, O.; McBride, J. R.; Tomlinson, I. D. Biocompatible Quantum Dots for Biological Applications. *Chem. Biol.* **2011**, *18*, 10−24.

(6) Buhbut, S.; Itzhakov, S.; Oron, D.; Zaban, A. Quantum Dot Antennas for Photoelectrochemical Solar Cells. *J. Phys. Chem. Lett.* **2011**, *2*, 1917−1924.

(7) Petryayeva, E.; Algar, W. R.; Medintz, I. L. Quantum Dots in Bioanalysis: A Review of Applications Across Various Platforms for Fluorescence Spectroscopy and Imaging. *Appl. Spectrosc.* **2013**, *67*, 215−252.

(8) Algar, W. R.; Kim, H.; Medintz, I. L.; Hildebrandt, N. Emerging Non-Traditional Förster Resonance Energy Transfer Configurations with Semiconductor Quantum Dots: Investigations and Applications. *Coord. Chem. Rev.* **2014**, *263−264*, 65−85.

(9) Algar, W. R.; Krull, U. J. New Opportunities in Multiplexed Optical Bioanalyses Using Quantum Dots and Donor-Acceptor Interactions. *Anal. Bioanal. Chem.* **2010**, *398*, 2439−2449.

(10) Geissler, D.; Charbonniere, L. J.; Ziessel, R. F.; Butlin, N. G.; Lohmannsroben, H. G.; Hildebrandt, N. Quantum Dot Biosensors for Ultrasensitive Multiplexed Diagnostics. *Ang. Chem., Int. Ed.* **2010**, *49*, 1396−1401.

(11) Medintz, I. L.; Mattoussi, H. Quantum Dot-Based Resonance Energy Transfer and its Growing Application in Biology. *Phys. Chem. Chem. Phys.* **2009**, *11*, 17−45.

(12) Morris-Cohen, A. J.; Frederick, M. T.; Cass, L. C.; Weiss, E. A. Simultaneous Determination of the Adsorption Constant and the Photoinduced Electron Transfer Rate for a Cds Quantum Dot Viologen Complex. *J. Am. Chem. Soc.* **2011**, *133*, 10146−10154.

(13) Huang, J.; Huang, Z.; Yang, Y.; Zhu, H.; Lian, T. Multiple Exciton Dissociation in CdSe Quantum Dots by Ultrafast Electron Transfer to Absorbed Methylene Blue. *J. Am. Chem. Soc.* **2010**, *132*, 4858−4864.

(14) Medintz, I. L.; Farrell, D.; Susumu, K.; Trammell, S. A.; Deschamps, J. R.; Brunel, F. M.; Dawson, P. E.; Mattoussi, H. Multiplex Charge Transfer Interactions Between Quantum Dots and Peptide-Bridged Ruthenium Complexes. *Anal. Chem.* **2009**, *81*, 4831−4839.

(15) Medintz, I. L.; Pons, T.; Trammell, S. A.; Grimes, A. F.; English, D. S.; Blanco-Canosa, J. B.; Dawson, P. E.; Mattoussi, H. Interactions between Redox Complexes and Semiconductor Quantum Dots Coupled via a Peptide Bridge. *J. Am. Chem. Soc.* **2008**, *130*, 16745−16756.

(16) Medintz, I. L.; Stewart, M. H.; Trammell, S. A.; Susumu, K.; Delehanty, J. B.; Mei, B. C.; Melinger, J. S.; Blanco-Canosa, J. B.; Dawson, P. E.; Mattoussi, H. Quantum-Dot/Dopamine Bioconjugates Function as Redox Coupled Assemblies for In Vitro and Intracellular pH Sensing. *Nat. Mater.* **2010**, *9*, 676−684.

(17) Aryal, B. P.; Benson, D. E. Electron Donor Solvent Effects Provide Biosensing with Quantum Dots. *J. Am. Chem. Soc.* **2006**, *128*, 15986−15987.

(18) Sandros, M. G.; Gao, D.; Benson, D. E. A Modular Nanoparticle-Based System for Reagentless Small Molecule Biosensing. *J. Am. Chem. Soc.* **2005**, *127*, 12198−12199.

(19) Swain, M. D.; Octain, J.; Benson, D. E. Unimolecular, Soluble Semiconductor Nanoparticle-Based Biosensors for Thrombin Using Charge/Electron Transfer. *Bioconjugate Chem.* **2008**, *19*, 2520−2526.

(20) Shete, V. S.; Benson, D. E. Protein Design Provides Lead(II) Ion Biosensors for Imaging Molecular Fluxes around Red Blood Cells. *Biochemistry* **2009**, *48*, 462−470.

(21) Opperwall, S. R.; Divakaran, A.; Porter, E. G.; Christians, J. A.; DenHartigh, A. J.; Benson, D. E. Wide Dynamic Range Sensing with Single Quantum Dot Biosensors. *ACS Nano* **2012**, *6*, 8078−8086.

(22) Callan, J. F.; Mulrooney, R. C.; Kamila, S.; McCaughan, B. Anion Sensing with Luminescent Quantum Dots - A Modular Approach Based on the Photoinduced Electron Transfer (PET) Mechanism. *J. Fluor.* **2008**, *18* (2), 527−532.

(23) Cui, S.-C.; Tachikawa, T.; Fujitsuka, M.; Majima, T. Solven-Polarity Dependence of Electron-Transfer Kinetics in a CdSe/ZnS Quantum Dot-Pyromellitimide Conjugate. *J. Phys. Chem. C* **2010**, *114*, 1217−1225.

(24) Matylistky, V. V.; Dworak, L.; Breus, V. V.; Basche, T.; Wachtveitl, J. Ultrafast Charge Separation in Multiexcited CdSe Quantum Dots Mediated by Adsorbed Electron Acceptors. *J. Am. Chem. Soc.* **2009**, *131*, 2424−2425.

(25) Sharma, S. N.; Pillai, Z. S.; Kamat, P. V. Photoinduced Charge Transfer between CdSe Quantum Dots and p-phenylenediamine. *J. Phys. Chem. B* **2003**, *107*, 10088−10093.
(26) Sykora, M.; Petruska, M. A.; Alstrum-Acevedo, J.; Bezel, I.; Meyer, T. J.; Klimov, V. I. Photoinduced Charge Transfer between CdSe Nanocrystal Quantum Dots and Ru-Polypyridine Complexes. *J. Am. Chem. Soc.* **2006**, *128*, 9984−9985.
(27) Juris, A.; Balzani, V.; Barigelletti, F.; Campagna, S.; Belser, P.; Vonzelewsky, A. Ru(II) Polypyridine Complexes - Photophysics, Photochemistry, Electrochemistry, and Chemi-luminescence. *Coord. Chem. Rev.* **1988**, *84*, 85−277.
(28) Trammell, S. A.; Goldston, H. M.; Tran, P. T.; Tender, L. W.; Conrad, D. W.; Benson, D. E.; Hellinga, H. W. Synthesis and Characterization of Ruthenium(II)-Based Redox Conjugate for Reagentless Biosensing. *Bioconjugate Chem.* **2001**, *12*, 643−647.
(29) Burda, C.; Green, T. C.; Link, S.; El-Sayed, M. A. Electron Shuttling Across the Interface of CdSe Nanoparticles Monitored by Femotsecond Laser Spectroscopy. *J. Phys. Chem. B* **1999**, *103*, 1783−1788.
(30) Dayal, S.; Burda, C. Suface Effects on Quantum Dot-Based Energy Transfer. *J. Am. Chem. Soc.* **2007**, *129*, 7977−7981.
(31) Huang, J.; Huang, Z.; Jin, S.; Lian, T. Exciton Dissociation in CdSe Quantum Dots by Hole Transfer to Phenothiazine. *J. Phys. Chem. C* **2008**, *112*, 19734−19738.
(32) Huang, J.; Stockwell, D.; Huang, Z.; Mohler, D. L.; Lian, T. Photoinduced Ultrafast Electron Transfer from CdSe Quantum Dots to Re-bipyridyl Complexes. *J. Am. Chem. Soc.* **2008**, *130*, 5632−5633.
(33) Tvrdy, K.; Frantsuzov, P. A.; Kamat, P. V. Photoinduced Electron Transfer from Semiconductor Quantum Dots to Metal Oxide Nanoparticles. *Proc. Nat. Acad. Sci.* **2011**, *108*, 29−34.
(34) Dabbousi, B. O.; Rodriguez-Viejo, J.; Mikulec, F. V.; Heine, J. R.; Mattoussi, H.; Ober, R.; Jensen, K. F.; Bawendi, M. G. (CdSe)ZnS Core-Shell Quantum Dots: Synthesis and Characterization of a Size Series of Highly Luminescent Nanocrystallites. *J. Phys. Chem. B* **1997**, *101*, 9463−9475.
(35) Susumu, K.; Oh, E.; Delehanty, J. B.; Blanco-Canosa, J. B.; Johnson, B. J.; Jain, V.; Hervey, W. J. H., IV; Algar, W. R.; Boeneman, K.; Dawson, P. E.; Medintz, I. L. Multifunctional Compact Zwitterionic Ligands for Preparing Robust Biocompatible Semiconductor Quantum Dots and Gold Nanoparticles. *J. Am. Chem. Soc.* **2011**, *133*, 9480−9496.
(36) Mei, B. C.; Susumu, K.; Medintz, I. L.; Delehanty, J. B.; Mountziaris, T. J.; Mattoussi, H. Modular poly(ethylene glycol) Ligands for Biocompatible Semiconductor and Gold Nanocrystals with Extended pH and Ionic Stability. *J. Mater. Chem.* **2008**, *18*, 4949−4958.
(37) Prasuhn, D. E.; Blanco-Canosa, J. B.; Vora, G. J.; Delehanty, J. B.; Susumu, K.; Mei, B. C.; Dawson, P. E.; Medintz, I. L. Combining Chemoselective Ligation with Polyhistidine-Driven Self-Assembly for the Modular Display of Biomolecules on Quantum Dots. *ACS Nano* **2010**, *4*, 267−278.
(38) Schnolzer, M.; Alewood, P.; Jones, A.; Alewood, D.; Kent, S. B. H. In Situ Neutralization in Boc-Chemistry Solid Phase Peptide Synthesis. *Int. J. Pept. Protein Res.* **1992**, *40*, 180−193.
(39) Sapsford, K. E.; Farrell, D.; Sun, S.; Rasooly, A.; Mattoussi, H.; Medintz, I. L. Monitoring of Enzymatic Proteolysis on a Electro-luminescent-CCD Microchip Platform Using Quantum Dot-Peptide Substrates. *Sensors Actuators B: Chem.* **2009**, *139*, 13−21.
(40) Goyne, K. W.; Brantley, S. L.; Chorover, J. Rare Earth Element Release from Phosphate Minerals in the Presence of Organic Acids. *Chem. Geol.* **2010**, *278*, 1−14.
(41) Ke, L.; Shilin, Z.; Jun, M. Study on Solubility of Cerium(IV) Phosphate. *J. Rare Earths* **2005**, *23*, 51−53.
(42) MaŠín, V.; Doležal, J. The Use of Cerium(IV) Phosphate for the Gravimetric Determination and Separation of Cerium. *Anal. Chim. Acta* **1978**, *101*, 413−418.
(43) Seim, K. L.; Obermeyer, A. C.; Francis, M. B. Oxidative Modification of Native Protein Residues Using Cerium(IV) Ammonium Nitrate. *J. Am. Chem. Soc.* **2011**, *133*, 16970−16976.
(44) Pons, T.; Medintz, I. L.; Wang, X.; English, D. S.; Mattoussi, H. Solution-Phase Single Quantum Dot Fluorescence Resonant Energy Transfer Sensing. *J. Am. Chem. Soc.* **2006**, *128*, 15324−15331.
(45) Stewart, M. H.; Huston, A.; Scott, A.; Oh, E.; Algar, W. R.; Deschamps, J.; Susumu, K.; Jain, V.; Prasuhn, D.; Blanco-Canosa, J.; Dawson, P.; Medintz, I. L. Competition Between FRET and Electron Transfer in Stoichiometrically-Assembled Quantum Dot-Fullerene Conjugates. *ACS Nano* **2013**, *7*, 9489−9505.
(46) Stewart, M. H.; Huston, A. L.; Scott, A. M.; Efros, A. L.; Melinger, J. S.; Gemmill, K. B.; Trammell, S. A.; Blanco-Canosa, J. B.; Dawson, P. E.; Medintz, I. L. Complex Förster Energy Transfer Interactions between Semiconductor Quantum Dots and a Redox-Active Osmium Assembly. *ACS Nano* **2012**, *6*, 5330−5343.
(47) Pettersen, E. F.; Goddard, T. D.; Huang, C. C.; Couch, G. S.; Greenblatt, D. M.; Meng, E. C.; Ferrin, T. E. UCSF Chimera − A Visualization System for Exploratory Research and Analysis. *J. Comput. Chem.* **2004**, *25*, 1605−1612.
(48) Boeneman, G. K.; Delehanty, J. B.; Blanco-Canosa, J.; Susumu, K.; Stewart, M. H.; Oh, E.; Huston, A. L.; Dawson, G.; Ingale, S.; Walters, R.; et al. Selecting Improved Peptidyl Motifs for Cytosolic Delivery of Disparate Protein and Nanoparticle Materials. *ACS Nano* **2013**, *7*, 3778−3796.
(49) Wang, J.; Wang, W.; Kollman, P. A.; Case, D. A. Automatic Atom Type and Bond Type Perception in Molecular Mechanical Calculations. *J. Mol. Graph.* **2006**, *25*, 247−260.
(50) Adzhubei, A. A.; Sternberg, M. J. E. Left-handed Polyproline II Helices Commonly Occur in Globular Proteins. *J. Mol. Biol.* **1993**, *229*, 472−473.
(51) Pons, T.; Medintz, I. L.; Sykora, M.; Mattoussi, H. Spectrally Resolved Energy Transfer Using Quantum Dot donors: Ensemble and Single-Molecule Photoluminescence Studies. *Phys. Rev. B* **2006**, *73*, 245302.
(52) Dennis, A. M.; Sotto, D.; Mei, B. C.; Medintz, I. L.; Mattoussi, H.; Bao, G. Surface Ligand Effects on Metal-Affinity Coordination to Quantum Dots: Implications for Nanoprobe Self-Assembly. *Bioconjugate Chem.* **2010**, *21*, 1160−1170.
(53) Sapsford, K. E.; Pons, T.; Medintz, I. L.; Higashiya, S.; Brunel, F. M.; Dawson, P. E.; Mattoussi, H. Kinetics of Metal-Affinity Driven Self-Assembly Between Proteins or Peptides and CdSe-ZnS Quantum Dots. *J. Phys. Chem. C* **2007**, *111*, 11528−11538.
(54) Blanco-Canosa, J.; Wu, M.; Susumu, K.; Petryayeva, E.; Jennings, T. L.; Dawson, P. E.; Algar, W. R.; Medintz, I. L. Recent Progress in the Bioconjugation of Quantum Dots. *Coord. Chem. Rev.* **2014**, *263*−*264*, 101−137.
(55) Adzhubei, A. A.; Sternberg, M. J.; Makarov, A. A. Polyproline-II Helix in Proteins: Structure and Function. *J. Mol. Biol.* **2013**, *425*, 2100−2132.
(56) Marshall, G. R.; Hodgkin, E. E.; Langs, D. A.; Smith, G. D.; Zabrocki, J.; Leplawy, M. T. Factor Governing Helical Preference of Peptides Containing Multiple α,α-dialkyl Amino Acids. *Proc. Natl. Acad. Sci. U.S.A.* **1990**, *87*, 487−491.
(57) Medintz, I. L.; Clapp, A. R.; Brunel, F. M.; Tiefenbrunn, T.; Uyeda, H. T.; Chang, E. L.; Deschamps, J. R.; Dawson, P. E.; Mattoussi, H. Proteolytic Activity Monitored by Fluorescence Resonance Energy Transfer Through Quantum-Dot-Peptide Conjugates. *Nat. Mater.* **2006**, *5*, 581−589.
(58) Prasuhn, D. E.; Deschamps, J. R.; Susumu, K.; Stewart, M. A.; Boeneman, K.; Blanco-Canosa, J. B.; Dawson, P. E.; Medintz, I. L. Polyvalent Display and Packing of Peptides and Proteins on Semiconductor Quantum Dots: Predicted Versus Experimental Results. *Small* **2009**, *6*, 555−564.
(59) Weiss, E. A. Organic Molecules as Tools to Control the Growth, Surface Structure, and Redox Activity of Colloidal Quantum Dots. *Acc. Chem. Res.* **2013**, *46*, 2607−2615.
(60) Zhu, H.; Song, N.; Lian, T. Controlling Charge Separation and Recombination Rates in CdSe/ZnS Type I Core-Shell Quantum Dots by Shell Thicknesses. *J. Am. Chem. Soc.* **2010**, *132*, 15038−15045.
(61) Winkler, J. R.; Gray, H. B. Electron Flow through Metalloproteins. *Chem. Rev.* **2013**, *114*, 3369−3380.

(62) McLaurin, E. J.; Greytak, A. B.; Bawendi, M. G.; Nocera, D. G. Two-Photon Absorbing Nanocrystal Sensor for Ratiometric Detection of Oxygen. *J. Am. Chem. Soc.* **2009**, *131*, 12994−13001.
(63) Byrne, A. G.; Burne, M. M.; Coker, G., III; Gemmill, K. B.; Spillmann, C.; Medintz, I. L.; Sloan, S. L.; van der Meer, B. W. Data. In *FRET - Förster Resonance Energy Transfer From Theory to Applications*; Medintz, I. L., Hildebrandt, N., Eds.; Wiley-VCH: Weinheim, 2013; pp 657−756.
(64) Norris, D. J.; Bawendi, M. G. StructureI the Lowest Absorption Feature of CdSe Quantum dots. *J. Chem. Phys.* **1995**, *193*, 5260−5268.
(65) Kambhampati, P.; Son, D. H.; Kee, T. W.; Barbara, P. F. Solvent Effects on Vibrational Coherence and Ultrafast Reaction Dynamics in the Multicolor Pump-Probe Spectroscopy of Intervalence Electron Transfer. *J. Phys. Chem. A* **2000**, *104*, 10637−10644.
(66) Bignozzi, C. A.; Argazzi, R.; Chiorboli, C.; Scandola, F.; Dyer, R. B.; Schoonover, J. R.; Meyer, T. J. Vibrational and Electronic Spectroscopy of Electronically Excited Polychromophoric Ruthenium (II) Complexes. *Inorg. Chem.* **1994**, *33*, 1652−1659.
(67) Turro, C.; Chung, Y. C.; Leventis, N.; Kuchenmeister, M. E.; Wagner, P. J.; Leroi, G. E. Resonance Raman Spectrum of the Phenanthroline Anion: Implications of Electron Delocalization in the MLCT Excited State of Ru(phen)32+. *Inorg. Chem.* **1996**, *35*, 5104−5106.
(68) Frederick, M. T.; Amin, V. A.; Weiss, E. A. Optical Properties of Strongly Coupled Quantum Dot-Ligand Systems. *J. Phys. Chem. Lett.* **2013**, *4*, 634−640.
(69) Evans, C. M.; Cass, L. C.; Knowles, K. E.; Tice, D. B.; Chang, R. P. H.; Weiss, E. A. Review of the Synthesis and Properties of Colloidal Quantum Dots: the Evolving Role of Coordinating Surface Ligands. *J. Coord. Chem.* **2013**, *65*, 2391−2414.
(70) Morris-Cohen, A. J.; Vasilenko, V.; Amin, V. A.; Reuter, M. G.; Weiss, E. A. Model for Adsorption of Ligands to Colloidal Quantum Dots with Concentration-Dependent Surface Structure. *ACS Nano* **2012**, *6*, 557−565.
(71) Iagatti, A.; Flamini, R.; Nocchetti, M.; Latterini, L. Photo-induced Formation of Bithiophene Radical Cation via a Hole-Transfer Process from CdS Nanocrystals. *J. Phys. Chem. C* **2013**, *117*, 23996−24002.
(72) Gill, R.; Zayats, M.; Willner, I. Semiconductor Quantum Dots for Bioanalysis. *Angew. Chem., Int. Ed.* **2008**, *47*, 7602−7625.
(73) Murphy, L. Biosensors and Bioelectrochemistry. *Curr. Opin. Chem. Biol.* **2006**, *10*, 177−184.
(74) Delehanty, J. B.; Boeneman, K.; Bradburne, C. E.; Robertson, K.; Medintz, I. L. Quantum Dots: A Powerful Tool for Understanding the Intricacies of Nanoparticle-Mediated Drug Delivery. *Expert Opin. Drug Delivery* **2009**, *6*, 1091−1112.
(75) Delehanty, J. B.; Mattoussi, H.; Medintz, I. L. Delivering Quantum Dots into Cells: Strategies, Progress and Remaining Issues. *Anal. Bioanal. Chem.* **2009**, *393*, 1091−1105.
(76) Biju, V.; Itoh, T.; Ishikawa, M. Delivering Quantum Dots to Cells: Bioconjugated Quantum Dots for Targeted and Nonspecific Extracellular and Intracellular Imaging. *Chem. Soc. Rev.* **2010**, *39*, 3031−3056.
(77) Goldman, E. R.; I.L, M.; Hayhurst, A.; Anderson, G. P.; Mauro, J. M.; Iverson, B. L.; Georgiou, G. M. H. Self-Assembled Luminescent CdSe-ZnS Quantum Dot Bioconjugates Prepared Using Engineered Poly-Histidine Terminated Proteins. *Anal. Chim. Acta* **2005**, *534*, 63−67.